Published online 15 April 2013

Nucleic Acids Research, 2013, Vol. 41, No. 11 ***e116***
doi:10.1093/nar/gkt230

Laser capture microdissection–reduced representation bisulfite sequencing (LCM-RRBS) maps changes in DNA methylation associated with gonadectomy-induced adrenocortical neoplasia in the mouse

Maximiliaan Schillebeeckx[1], Anja Schrade[2,3,4,5], Ann-Kathrin Löbs[2,3,4], Marjut Pihlajoki[2,3,5], David B. Wilson[2,3] and Robi D. Mitra[1,*]

[1]Department of Genetics, Center for Genome Sciences, Washington University School of Medicine, 4444 Forest Park Parkway, St. Louis, Missouri 63110, USA, [2]Department of Pediatrics, St. Louis Children's Hospital, Washington University School of Medicine, 660 S. Euclid Ave., St. Louis, Missouri 63110, USA, [3]Department of Developmental Biology, Washington University School of Medicine, 660 S. Euclid Ave., St. Louis, Missouri 63110, USA, [4]Department of Biotechnology, Hochschule Mannheim, University of Applied Sciences, Paul-Wittsack-Straße 10, 68163 Mannheim, Germany and [5]Department of Pediatrics, University of Helsinki, Biomedicum Helsinki 2U, Tukholmankatu 8, 00014 Helsinki, Finland

Received July 30, 2012; Revised March 12, 2013; Accepted March 13, 2013

ABSTRACT

DNA methylation is a mechanism for long-term transcriptional regulation and is required for normal cellular differentiation. Failure to properly establish or maintain DNA methylation patterns leads to cell dysfunction and diseases such as cancer. Identifying DNA methylation signatures in complex tissues can be challenging owing to inaccurate cell enrichment methods and low DNA yields. We have developed a technique called laser capture microdissection-reduced representation bisulfite sequencing (LCM-RRBS) for the multiplexed interrogation of the DNA methylation status of cytosine–guanine dinucleotide islands and promoters. LCM-RRBS accurately and reproducibly profiles genome-wide methylation of DNA extracted from microdissected fresh frozen or formalin-fixed paraffin-embedded tissue samples. To demonstrate the utility of LCM-RRBS, we characterized changes in DNA methylation associated with gonadectomy-induced adrenocortical neoplasia in the mouse. Compared with adjacent normal tissue, the adrenocortical tumors showed reproducible gains and losses of DNA methylation at genes involved in cell differentiation and organ development. LCM-RRBS is a rapid, cost-effective, and sensitive technique for analyzing DNA methylation in heterogeneous tissues and will facilitate the investigation of DNA methylation in cancer and organ development.

INTRODUCTION

DNA methylation has long been recognized to play a role in normal cellular differentiation and development. Methylation most often occurs at the cytosine of a cytosine–guanine dinucleotide (CpG) and acts to down-regulate gene expression (1). Disruption of the DNA methylation machinery can lead to imprinting disorders (2), repeat-instability disease (3) and neurological defects (4,5).

DNA methylation has been shown to play an important role in cancer progression. Tumors often display a global loss of methylation, or hypomethylation, at repetitive elements, which is thought to destabilize the genome through transposon-mediated rearrangements (6,7), activate growth-promoting oncogenes (7) and cause de-differentiation through the loss of imprinting (8). An abnormal gain of methylation, or hypermethylation, at gene regulatory elements also contributes to tumorigenesis by silencing tumor suppressor genes involved in DNA damage repair, cell cycle control and other processes (9). This aberrant methylation may be due, at least in part, to recurring mutations in genes that are involved in epigenetic regulation (10,11), such as DNA methyltransferases,

*To whom correspondence should be addressed. Tel: +1 314 362 2751; Fax: +1 314 362 7855; Email: rmitra@genetics.wustl.edu

which are commonly mutated in acute myeloid leukemia (12), and chromatin remodelling enzymes, which are frequently mutated in renal carcinomas and pancreatic neuroendocrine tumors (13,14).

Accurate analysis of DNA methylation is complicated by the heterogeneous nature of normal and diseased tissues. Normal tissues contain cells at different stages of differentiation/maturity. Tumors also consist of histologically diverse cell types (15,16) and display intratumor heterogeneity in gene expression (17), genotype (18,19) and metastatic and proliferative potential (20,21). Therefore, the analysis of gross tumor samples often obscures the diverse cell types that comprise the entire tumor (22). To assess cell type–specific DNA methylation of complex tissues, cell isolation techniques must be used. Laser capture microdissection (LCM) has enabled researchers to separate specific cell types from heterogeneous tissues (23). DNA yields from such samples, however, are too small to use with current methods for genome-wide DNA methylation analysis. Moreover, clinical samples are typically fixed in formalin and embedded in paraffin, further compromising DNA quality. For these reasons, the genome-wide mapping of DNA methylation in LCM samples has not been previously demonstrated.

Current DNA methylation analysis methods are limited by the number of loci interrogated, quantity and quality of DNA input required, and sample throughput (24). Methods that function on a very small number of cells interrogate only a few genomic loci and are challenging to implement (25,26). Furthermore, few methods function on clinical samples that are formalin-fixed and paraffin-embedded (FFPE) (26). Genome-wide DNA methylation methods are limited by the input of DNA. Affinity enrichment techniques like MeDIP-Seq (27), MDB-seq (28) and MethylCap-seq (29) require 0.16–5 μg of DNA input and are limited to a 150- to 200-bp resolution. Other global methods, like CHARM (30) and padlock probes (31,32), also require large DNA inputs. MethylC-seq, the only truly whole-genome approach (33), is prohibitively expensive when many samples need to be analyzed. Reduced representation bisulfite sequencing (RRBS) can map genome-wide DNA methylation of limited DNA samples (34), but has not been demonstrated to function on small amounts of DNA recovered from FFPE samples or on samples collected by LCM.

Here, we describe a new technique termed laser capture microdissection-reduced representation bisulfite sequencing (LCM-RRBS) that can interrogate genome-wide DNA methylation patterns in samples collected from complex heterogeneous tissues. As a proof of principle, we have used LCM-RRBS to analyze global DNA methylation changes associated with adrenocortical neoplasia in the mouse. In response to gonadectomy (GDX) and the ensuing rise in serum gonadotropin levels, sex steroid–producing neoplasms accumulate in the subcapsular region of the adrenal cortex of certain strains of mice, including DBA/2J (35). This phenomenon is thought to reflect gonadotropin-induced metaplasia of stem/progenitor cells in the adrenal cortex, although the term 'neoplasia' is used more often than 'metaplasia' to describe the process (35). The molecular basis of GDX-induced adrenocortical neoplasia is unknown (36,37), but it has been hypothesized that DNA methylation and other epigenetic modifications may impact the phenotypic plasticity of adrenocortical stem/progenitor cells, allowing them to respond to the rise in circulating gonadotropins (38). GDX-induced adrenocortical neoplasia in the mouse is an ideal phenomenon to study using LCM-RRBS because of the limited amounts of tissue that can be collected.

MATERIALS AND METHODS

Experimental mice

Procedures involving mice were approved by an institutional committee for laboratory animal care and were conducted in accordance with NIH guidelines for the care and use of experimental animals. C57BL/6J and DBA/2J mice were purchased from Jackson Laboratories (Bar Harbor, ME). Mice were anesthetized and ovariectomized at 3–4 weeks of age (39).

DNA extraction

Human tumor specimens were collected under an institutional review board–approved protocol. Immediately after surgery, a human endometrial tumor was divided in half. One half was fresh frozen, whereas the other was formalin fixed and paraffin embedded (FFPE). Fifty milligrams of fresh frozen endometrial tumor was cut into small pieces with a sterile scalpel blade, and DNA extracted using the Maxwell 16 Tissue DNA Purification Kit (AS1030, Promega). The FFPE preserved portion was cut into 6-μm sections onto microscope slides. Four 4-mm^2 slices were scratched off the slide with a sterile scalpel blade and combined in 80 μl of buffer and proteinase K (740901.50, Clontech) and incubated overnight at 65°C. Liver tissue was harvested from C57BL/6J mice and divided in half. One half was preserved in Tissue-tek optimal cutting temperature (O.C.T.) compound (25608-930, VWR) and snap frozen, whereas the other half was FFPE for downstream bulk DNA extraction and LCM. Fresh frozen, FFPE and LCM samples were purified using NucleoSpin Tissue XS columns (740901.5, Clontech) following the protocol for laser-microdissected tissue and eluted in 20 μl of nuclease-free water. Genomic DNA was quantified using the Quant-it dsDNA High-Sensitivity kit (Invitrogen) and the Qubit fluorometer (Invitrogen).

Laser capture microdissection

Adrenal glands were harvested from mice 3 months after ovariectomy. Liver and adrenal cryosections (10 μm) were collected on membrane slides (PEN-Membrane 2.0 μm; Leica) designed to free the dissectate from the remainder of the tissue section. Adrenal tissue sections were fixed in acetone (5 s, −20°C), stained with hematoxylin and eosin (H&E) or crystal violet and dehydrated by passage through successively higher concentrations of ethanol followed by xylene. FFPE liver sections were

deparaffinized and dehydrated using standard methods. LCM was performed using a Leica LMD6000 microscope. Dissectates were collected in SDS/proteinase K for genomic DNA isolation (740901.5, Clontech).

RRBS and LCM-RRBS

RRBS was performed on 400 ng of commercially purchased leukocyte genomic DNA (D1234148, Amsbio) and genomic DNA extracted from a mouse liver as previously described (40). For LCM-RRBS, leukocyte genomic DNA (1 ng), extracted endometrial tumor genomic DNA (1 ng) and LCM DNA samples were incubated overnight at 37°C with 20 U of the methylation-insensitive restriction enzyme MspI (R0106S, NEB) and 2 µl of 10× NEBuffer 2 in an 18-µl reaction. Without subsequent purification, fragment ends were filled in, and an adenosine added with 10 U of Klenow Fragment (3′ → 5′ *exo*$^-$, M0212L, NEB), 0.04 mM dGTP, 0.04 mM dCTP, 0.4 mM dATP and 1× NEBuffer 2 to a final volume of 22.4 µl. The reaction was incubated at 30°C for 20 min, 37°C for 20 min, and 75°C for 20 min. Pre-annealed methylated paired-end Illumina indexing adapters (Adap1: ACACTCTTTCCCTACACGACGCTCTTCC GATCT; Adap2: P-GATCGGAAGAGCACACGTCTG AACTCCAGTCAC, P = phosphate) at a concentration of 0.26 mM were ligated overnight at 16°C to the ends of the DNA fragments using 1200 U of T4 DNA Ligase (M0202L, NEB) in 1× Ligase Buffer to a final volume of 28.9 µl. These adapter oligonucleotides are only complementary at 13 bases, which, after annealing, form a 'Y' structure. Because excess adapters prevent the complete conversion of CpGs at the MspI digestion site, adapter-ligated fragments are purified using MinElute columns (Qiagen) and eluted twice with 11 µl of warm EB buffer (Qiagen). The purified products were treated using the EZ DNA Methylation Gold Kit (D5005, Zymo). Samples were eluted in 11 µl of M-Elution buffer. To incorporate the sample-specific index, 3 µl of each bisulfite-treated sample was amplified in triplicate with 0.2 µM of indexed primers (PCR1: AATGATACGGCGACCACC GAGATCTACACTCTTTCCCTACACGACGCTCTTC CGATCT; PCR2: CAAGCAGAAGACGGCATACGA GATNNNNNGTGACTGGAGTTCAGACGTGTGCT CTTCCGA, N = index), 5 U of Platinum Taq Polymerase (10966-034, Invitrogen), 1× PCR buffer, 2 mM $MgCl_2$, 0.5 M betaine (B0300, Sigma) and 1 mM dNTP, in a 10-µl reaction using the following cycling conditions: 98°C for 2 min, 12 cycles of 98°C for 30 s and 65°C for 2 min. All PCR products and replicates were pooled and analyzed by electrophoresis on a 3% 1× Tris-acetate-EDTA NuSieve agarose gel (50090, Lonza) using a voltage of 5 V/cm until the blue loading dye was 6–7 cm away from the loading well. Fragments between 150 and 350 bp were extracted and purified using MinElute columns (Qiagen) and 15 µl of warmed EB buffer. Before final library PCR enrichment, the minimum cycle number must be determined to ensure no PCR bias. Using 2 µl of eluted product and 0.2 µM universal primers (Pool1: CAAGCAGAAGACGGCATACGAG AT, Pool2: AATGATACGGCGACCACCGAGATCT), multiple PCR reactions with a final volume of 50 µl are set up using the previous conditions but varying the cycle number from 10 to 16 cycles. Ten microliters of each PCR product is analyzed through electrophoresis on a 4–20% Precast Tris-borate-EDTA (TBE) gel (3450059, BioRad) and stained with Sybr Gold (S-11494, Invitrogen) for 15 min and imaged. To minimize PCR bias, the final PCR library is amplified in quadruplicate using the previous PCR conditions and the minimum cycle number (typically ~14) that shows amplification only within the 150- to 350-bp range on the Sybr Gold–stained TBE gel. The four replicates are pooled and gel extracted as previously mentioned to remove remaining adapter dimers and primers, purified and sequenced on Illumina HiSeq 2000 machines.

Bisulfite-specific PCR

Neoplastic and adjacent normal mouse adrenocortical tissue was collected and bisulfite treated using the EZ DNA Methylation-Direct kit following the manufacturer's instructions for LCM samples eluting with 15 µl of nuclease-free water (D5020, Zymo). Bisulfite-specific PCR (BSP) primers were designed using MethPrimer (http://www.urogene.org/methprimer/). To amplify the promoter regions of interest, 2 µl of bisulfite-treated DNA was combined with 2.5 U of Jumpstart Taq (Sigma), 1× PCR buffer, 1 M betaine (B0300, Sigma), 0.2 mM dNTP and 0.4 µM of each primer in a total reaction volume of 25 µl. The reaction was incubated at 95°C for 5 min, followed by 5 cycles at 94°C for 30 s, 60°C for 30 s and 72°C for 90 s, followed by 5 cycles at 94°C for 30 s, 55°C for 30 s and 72°C for 90 s, followed by 30–33 cycles at 94°C for 30 s, 50°C for 30 s and 72°C for 90 s, followed by incubation at 72°C for 5 min. PCR products were prepared for sequencing on the MiSeq following the manufacturer's protocol (Illumina).

Sequence alignment and methylation calling

All analysis was performed using the February 2009 (GrCh37/hg19) build of the human genome and the July 2007 (NCBI37/mm9) build of the mouse genome. On average, 25 million single-end 42-bp raw high-quality reads per sample were either aligned to the cytosine-poor strand reference using the bisulfite mode of MAQ (41) or aligned to the reduced reference using RRBSMAP (42) filtering against reads that contain adapter sequence. Reads that showed <90% bisulfite conversion (approximately one unconverted non-CpG cytosine per read) were filtered to remove those that resulted from incomplete bisulfite-converted molecules. Aligned reads with a mapping quality of zero were also discarded. The resulting high-quality uniquely mapped reads were used for methylation calling. We identified the genomic coordinates of all CpGs in the reference sequence and assessed percent DNA methylation by calculating the fraction of reads that had an unconverted cytosine at the CpG position relative to the total reads. We required that each read have either a 'TG' or 'CG' dinucleotide at the expected CpG coordinate to be considered for analysis.

Genomic feature annotation and statistical analysis

Cytosine methylation levels were determined for two classes of genomic features downloaded from the UCSC genome browser (43). CpG islands (CGIs) were defined as a region >200 bp with a GC content of 50% or greater and observed-to-expected ratio of CG dinucleotides >0.6 (44). Promoters were defined as a 2-kb region centered on the annotated transcription start site (TSS) of RefSeq genes (45). For LCM-RRBS, RRBS, fresh frozen and FFPE comparisons, only genomic features with at least 50 methylation measurements in each pairwise comparison were considered for analysis.

To identify differentially methylated promoters in adrenocortical neoplasia and normal samples, the DNA methylation status of all CpGs within a 2-kb region of all RefSeq annotated TSSs were compared. Those promoters with at least 50 methylation measurements that showed >10% methylation difference were considered for statistical analysis. Promoters were considered statistically significant with a $P < 0.05$ using Student's *t*-test after *P*-values were adjusted using a false-discovery rate (FDR) of 5%. Statistical significance across BSP samples was determined using the Fisher's exact test. All statistical analysis was performed using R.

Data release

The DNA methylation data generated for this study can be found under the NCBI Gene Expression Omnibus (GEO) accession number GSE 45361. DNA methylation and raw sequence data are also publically available at the Center for Genome Sciences (www.cgs.wustl.edu/~maxim/).

RESULTS

LCM-RRBS

RRBS is an established methylation analysis method that can interrogate most CGIs and promoters across the entire genome. Current RRBS protocols, however, do not allow for multiplexing and have not been demonstrated on samples isolated by LCM. Furthermore, although RRBS has been used to analyze small amounts of high-quality DNA (34), it has not been applied to <1 μg of DNA extracted from FFPE samples (46), the most common method used to preserve clinical tissue samples. We therefore sought to develop a method to analyze small amounts (1 ng) of DNA from laser capture microdissected samples and from FFPE-preserved samples, and to interrogate multiple samples in parallel.

Our protocol removes most clean-up steps, which ensures DNA samples are not lost, and leverages the capabilities of Illumina indexing to pool samples before size selection and sequencing, thus dramatically increasing the number of samples that can be processed in parallel (Figure 1). LCM-RRBS digests genomic DNA with MspI to create fragments with a 5′-CpG end. Digested fragments are blunted, adenylated and ligated with methylated sequencing adapters and then column purified to remove excess adapters. To convert the epigenetic methylation mark into a genetic mark that can be read through genomic sequencing, adapter-ligated fragments are treated with bisulfite. At this stage, converted DNA is amplified with a low-cycle PCR to introduce sample-specific indexes. Once each sample is 'indexed', samples are pooled before gel electrophoreses and the isolation of 40- to 220-bp fragments. The purified pooled library is PCR enriched using universal primers and sequenced on the Illumina platform to generate 42-bp reads. Using our modified method, we can interrogate CpGs genome-wide from laser capture microdissected samples freshly frozen or previously preserved through formalin fixing and paraffin embedding.

LCM-RRBS accurately measures genome-wide DNA methylation of fresh frozen and FFPE samples

To evaluate the performance of LCM-RRBS, we benchmarked it against RRBS. Using 1 and 400 ng for LCM-RRBS and RRBS, respectively, we compared the genome-wide DNA methylation status of DNA isolated from human blood leukocytes. We did not do LCM on the 1 ng of purified DNA; instead, we only applied the downstream library preparation of the LCM-RRBS protocol (Figure 1). LCM-RRBS was able to interrogate >75% of CGIs and >65% of gene promoters, results that were similar to those obtained by RRBS (Supplementary Figure S1). LCM-RRBS was able to accurately measure the DNA methylation levels of CGIs and core promoters (Figure 2A) as well as individual CpG dinucleotides (Supplementary Figure S2). Increasing the required coverage for each CpG considered for CGI methylation did not significantly alter the concordance between RRBS and LCM-RRBS (Supplementary Figure S3). For CGIs ($n = 18\,448$) and promoters ($n = 8500$) having at least 50 methylation measurements, we observed a Pearson correlation of 0.98 and 0.94, respectively, between 1 and 400 ng (Figure 2A). Most CGIs are either highly methylated (80–100%) or highly unmethylated (0–20%). We therefore sought to test how well LCM-RRBS could call a CGI as methylated or unmethylated. For CGIs with at least 50 high-quality CpG measurements, LCM-RRBS identified methylated CGIs with 91% sensitivity and 99% specificity and unmethylated CGIs with 97% sensitivity and 94% specificity when compared with the RRBS dataset. We therefore conclude that LCM-RRBS functions on as little as 1 ng of genomic DNA, interrogates most CGIs and promoters and is very accurate.

Human clinical samples are usually stored as either fresh frozen or FFPE specimens. Mapping DNA methylation in the latter, however, can be challenging because formalin fixation degrades DNA. Most DNA methylation techniques that have been used on FFPE samples require >1 μg of DNA or can only interrogate a few loci. To validate the reproducibility of LCM-RRBS and demonstrate its universal clinical applicability, we performed methylation profiling on 1-ng samples of DNA from a primary endometrial carcinoma, half of which was fresh frozen and the remainder which was FFPE preserved. Methylation of CGIs and promoters was highly concordant between fresh frozen and FFPE samples (Pearson correlation 0.98 and 0.97, respectively; Figure 2B). CGI and

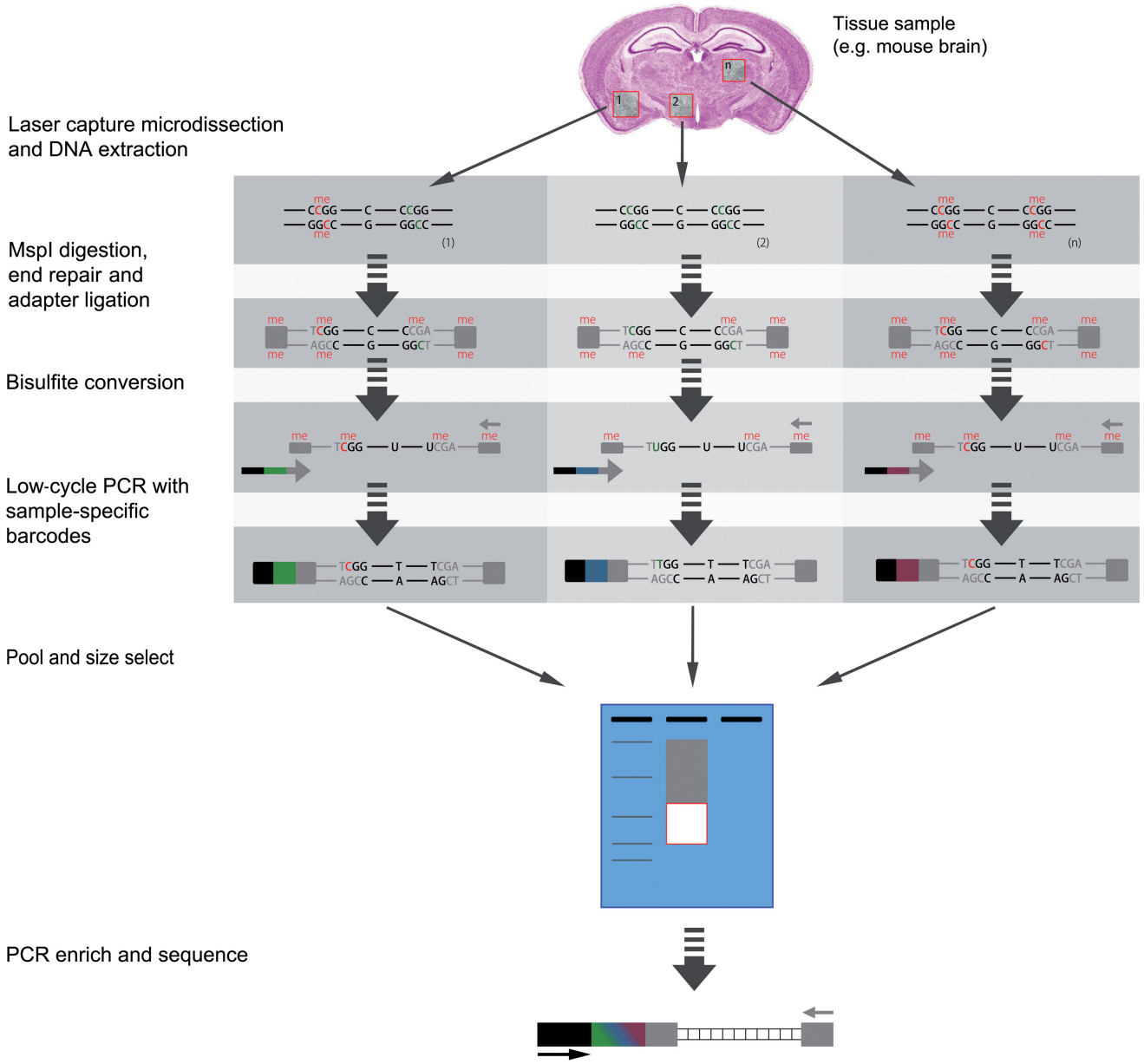

Figure 1. LCM-RRBS workflow. A complex tissue is dissected using LCM. Extracted DNA is digested by the methylation-insensitive enzyme MspI, end repaired and ligated with methylated Illumina adapters. After bisulfite conversion, each sample is 'barcoded' by introducing a sample-specific index (shown as green, blue or violet boxes) through low-cycle PCR. Samples are pooled and loaded onto a high-percentage gel for fragment separation and size selection. Using universal primers, the final library is amplified and sequenced on the Illumina platform.

promoter methylation correlated strongly between FFPE technical replicates (Pearson correlation 0.97 and 0.95, respectively; Supplementary Figure S4). We also observed high concordance across individual CpGs between fresh frozen and FFPE tumor samples, with a Pearson correlation of 0.96 (Supplementary Figure S2). LCM-RRBS, therefore, can accurately interrogate genome-wide methylation of 1 ng extracted from FFPE samples.

LCM-RRBS is robust across fresh frozen and FFPE laser capture microdissected samples

In situ analysis of DNA methylation is challenging owing to the heterogeneous nature of complex tissues. To interrogate only cells of interest in biological and clinical samples, LCM techniques must be used to enrich for a specific cell type. Current genome-wide DNA methylation methods, however, have not been demonstrated to function on LCM-collected samples. We therefore set out to evaluate the performance of LCM-RRBS on fresh frozen and FFPE samples collected by LCM.

Because the cellular architecture of a normal liver is homogeneous, the methylation state should be very similar throughout the organ. Thus, the liver serves as the ideal tissue for benchmarking the LCM-RRBS method against the RRBS gold standard, as each microdissected region should have a very similar

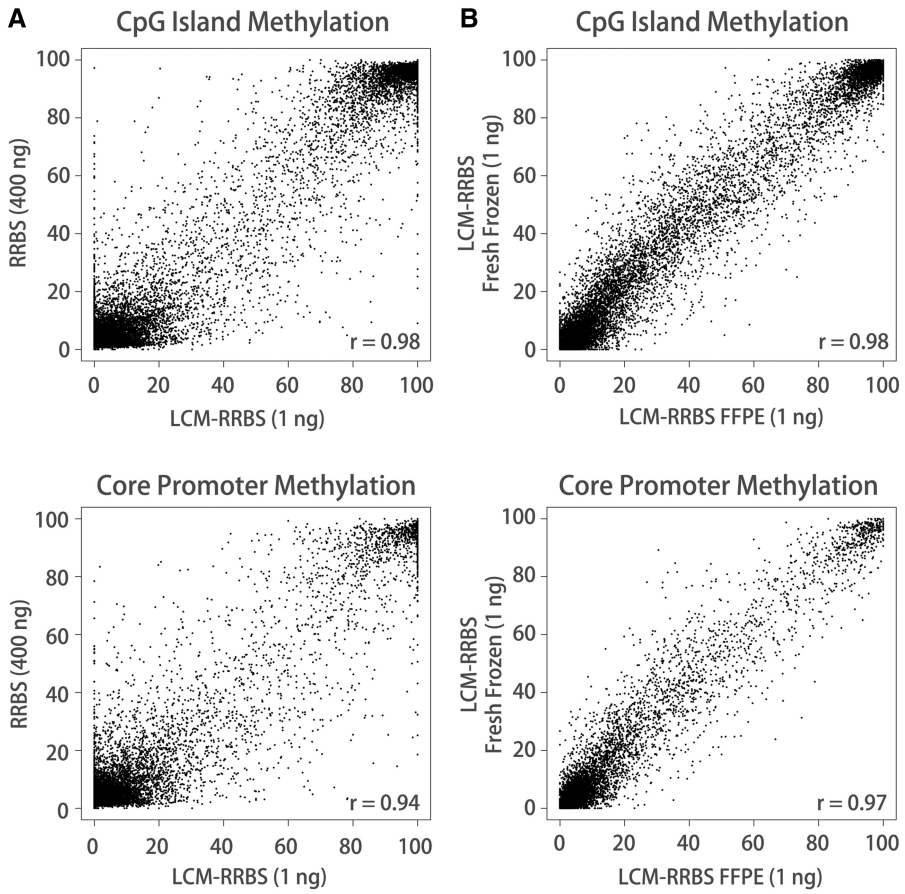

Figure 2. LCM-RRBS is reproducible and robust across 1 ng extracted from bulk fresh frozen and FFPE samples. CGI methylation (top panels) and the methylation at 2-kb regions flanking the TSS (bottom panels) were compared between (**A**) 1 ng (LCM-RRBS) and 400 ng of purified leukocyte genomic DNA (RRBS), and (**B**) 1 ng of FFPE DNA and 1 ng of fresh frozen genomic DNA extracted from the same endometrial tumor (LCM-RRBS).

methylation pattern to that of the bulk tissue. We harvested the liver of C57BL/6J mice and prepared the liver using standard preservation techniques. Separate regions of the liver were either directly snap frozen, preserved in Tissue-Tek O.C.T. compound and then snap frozen or preserved using formalin fixation and paraffin embedding. Bulk DNA was extracted from the snap-frozen sample and used for downstream RRBS analysis. To determine whether the process of LCM alters the methylation of DNA and to assess the lower limits of LCM-RRBS, we applied LCM-RRBS to samples collected from 20, 10, 5 and 2 mm^2 of the fresh frozen and FFPE mouse liver and compared the DNA methylation patterns with those determined by performing RRBS on 400 ng of DNA extracted from the bulk fresh frozen liver tissue. As observed with 1 ng of DNA, most CGIs and promoters were represented even when only 2 mm^2 of tissue was collected (Supplementary Figure S5). Furthermore, CGI (mean Pearson = 0.98) and promoter (mean Pearson = 0.96) methylation showed high concordance across all fresh frozen samples (Figure 3A) when compared with 400 ng of DNA. For samples collected from 2 mm^2 of microdissected tissue, LCM-RRBS identified unmethylated (0–20%) CGIs with 88% sensitivity and 99% specificity and methylated (80–100%) CGIs with 99% sensitivity and 87% specificity. While the interrogation of DNA methylation of 2 mm^2 of fresh frozen tissue was robust, 20 mm^2 of FFPE tissue was required for accurate analysis. Using 20 mm^2 of FFPE starting material, LCM-RRBS showed 79% sensitivity and 99% specificity for calling unmethylated (0–20%) CGIs and 99% sensitivity and 78% specificity for calling methylated (80–100%) CGIs, with a Pearson correlation of 0.95 (Figure 3B). Samples collected from <20 mm^2 of FFPE tissue, however, showed poor CGI, promoter and CpG correlations as compared with 400 ng (data not shown). We conclude that the process of LCM does not alter DNA methylation, and that LCM-RRBS accurately determines methylation patterns from as little as 2 mm^2 of fresh frozen tissue. FFPE tissue is more problematic, requiring an area of at least 20 mm^2 to achieve acceptable, but not exceptional, performance.

Evaluation of PCR bias

PCR amplification of small amounts of bisulfite-treated DNA can result in PCR bias and inaccurate DNA methylation calling (47). In DNA samples obtained from females, the X chromosome serves as a good internal

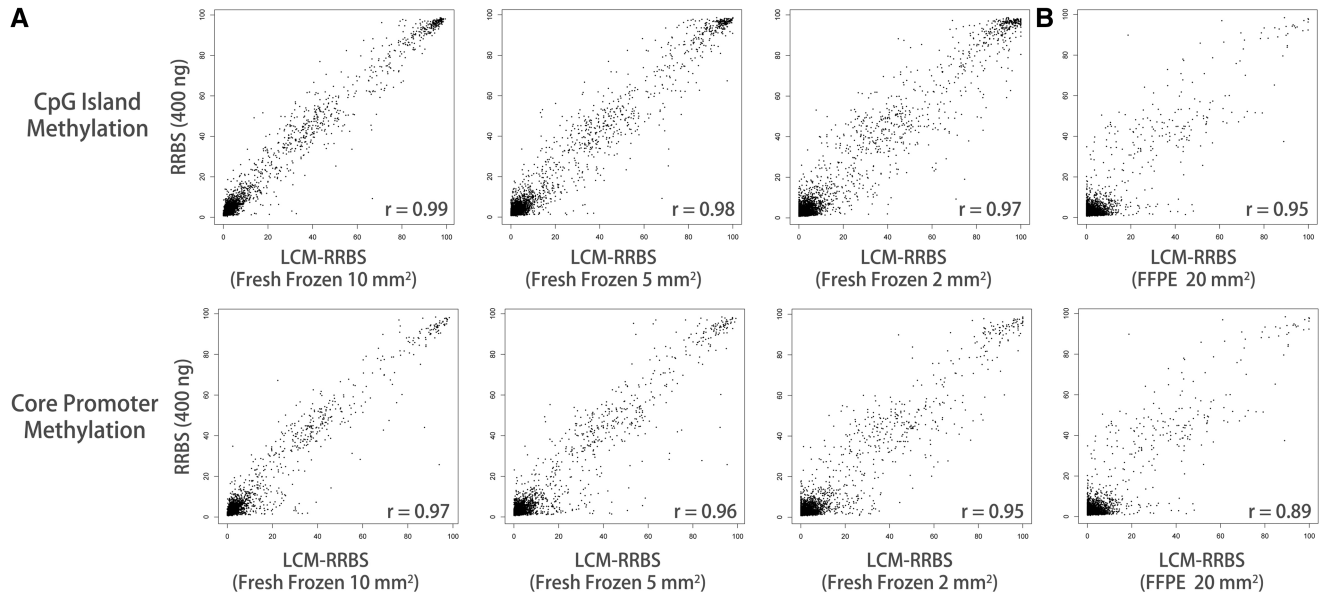

Figure 3. LCM-RRBS is robust across microdissected samples collected from fresh frozen and FFPE tissues. Fresh frozen and FFPE mouse liver was collected for DNA methylation profiling. LCM was used to collect tissue from areas ranging in size from 20 to 2 mm^2. CGI methylation (top panels) and methylation at 2-kb regions flanking the TSS (bottom panels) were compared between (**A**) fresh frozen samples (LCM-RRBS) and 400 ng of purified mouse liver genomic DNA (RRBS), and (**B**) FFPE samples (LCM-RRBS) and 400 ng of purified mouse liver genomic DNA (RRBS).

control for assessing PCR bias, as X inactivation methylates one copy of the X chromosome at most loci. To determine whether LCM-RRBS suffers from PCR bias, we analyzed the fraction of molecules that were methylated at loci known to be affected by X inactivation. As expected, the majority (>70%) of CGIs on the X chromosome showed an intermediate level (30–70%) of DNA methylation across all fresh frozen samples and the 20-mm^2 FFPE sample (Supplementary Figure S6), demonstrating that LCM-RRBS shows little PCR bias. We conclude that LCM-RRBS shows little PCR bias across 2 mm^2 of fresh frozen tissue and 20 mm^2 of FFPE tissue.

Analysis of GDX-induced adrenocortical neoplasia in the mouse using LCM-RRBS

To demonstrate the utility of LCM-RRBS in a biological setting, we applied the method to analyze the DNA methylation of neoplasms that arise in the adrenal cortex of DBA/2J mice after GDX. Although genetic factors have been identified that influence susceptibility to GDX (36,37), little is known about the role DNA methylation plays in the formation of GDX-induced neoplasia. Molecular characterization is further complicated because mouse adrenal glands are only 0.1 cm^2 in size and neoplasms arise among normal tissues, requiring LCM enrichment methods for tissue isolation. We therefore applied LCM-RRBS to neoplastic and adjacent normal mouse adrenal tissues (Figure 4).

In one multiplexed experiment, we interrogated the methylation status of >13 000 promoters and >13 000 CGIs of six tissue samples (three neoplastic and three normal representing three different mice), across an average of >800 000 CpGs per sample (Figure 4 and Supplementary Table S1). Using a threshold difference of at least 10%, 37 promoters were significantly hypomethylated and 8 promoters were significantly hypermethylated ($P < 0.05$, FDR adjusted; Table 1 and Supplementary Table S2) in the neoplasms compared with adjacent normal tissue. Many of the top hypo- and hypermethylated genes have been implicated in cell fate determination and differentiation, including adrenocortical formation (*Tinagl1*), gonad development (*Foxs1*, *Wdr63*, *Tmem184a*), pancreas development (*Nsmce1*), kidney development (*Hoxc10*, *Dpep1*), prostate development (*Il17rc*, *Ano7*) and muscle and skeletal development (*Myo18b*, *Trim63*, *Lmod3*, *Meox1*). The observed methylation changes suggest the neoplastic tissue may arise owing to aberrant gene expression of genes normally silent in adrenocortical cells or the silencing of adrenal-specific markers. To validate our findings, we performed bisulfite-specific PCR (BSP) followed by sequencing of three hypomethylated promoters and one hypermethylated promoter on neoplastic and normal tissues isolated by LCM. For all promoters tested, BSP showed a significant difference (Fisher's exact test, $P < 10^{-15}$) in DNA methylation between the neoplasia and normal tissue as predicted by LCM-RRBS (Figure 5). Taken together, these results demonstrate that LCM-RRBS can identify differentially methylated genes in a complex tissue and reveal functionally relevant epigenetic effects.

DISCUSSION

Current DNA methylation mapping techniques are limited by input and the number of loci interrogated. RRBS, a genome-wide DNA methylation mapping

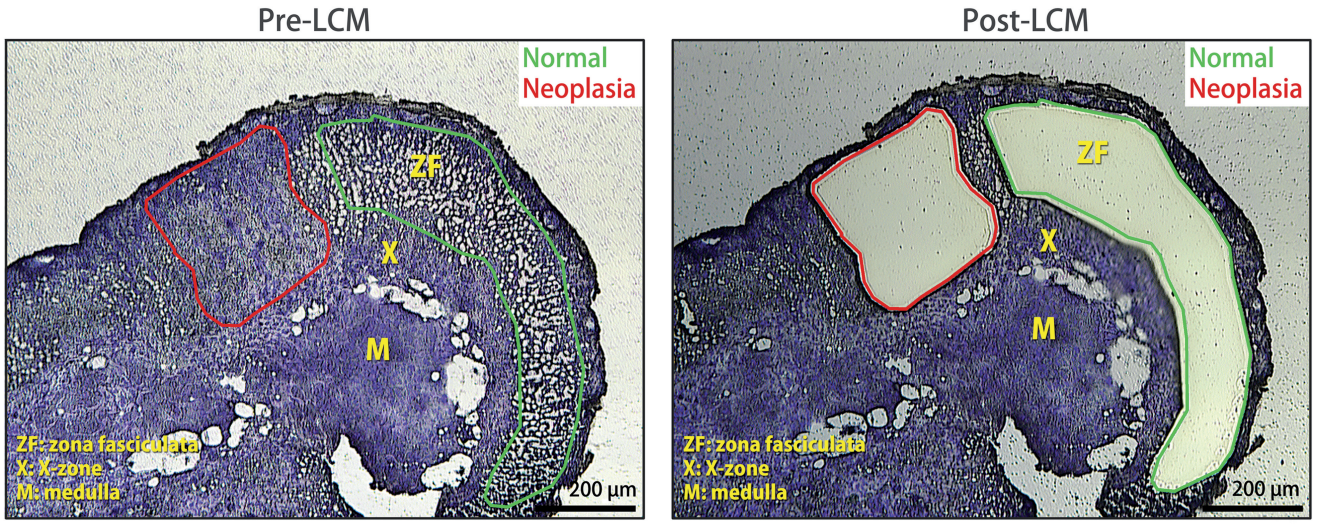

Figure 4. DNA methylation profiling of GDX-induced adrenocortical neoplasms and adjacent normal tissue using LCM-RRBS. The adrenal glands of three ovariectomized DBA/2J mice were fresh frozen in Tissue-tek O.C.T. compound, cryosectioned and stained. Shown are representative cryosections pre- and post-LCM. Normal cells in the zona fasciculata contain large lipid droplets that are easily recognized. In contrast, neoplastic cells distort the normal adrenal zonal architecture and contain relatively few lipid droplets. The microdissected normal tissue included zona glomerulosa and zona fasciculata cells; care was taken to avoid dissection of X-zone (X), medulla (M) or capsule cells, as these cell types have distinct developmental origins (48), and therefore may have different epigenetic fingerprints. An average of 5.5 mm^2 of neoplastic (red) and normal (green) tissue per adrenal pair was collected and analyzed using LCM-RRBS.

Table 1. Top hypermethylated and hypomethylated genes in GDX-induced adrenocortical neoplasms of the mouse

Gene symbol	Entrez gene name	Function[a]	Percent methylation[b]			*P* value[c]
			Normal	Neoplasia	Difference	
Tinagl1	Tubulointerstitial nephritis antigen-like 1	Zonal differentiation of adrenocortical cells	18	64	46	0.0235
Dennd4b	DENN/MADD domain containing 4B	unknown	34	62	29	0.0125
L1td1	LINE-1 type transposase domain containing 1	Embryonic stem cell renewal and identity	33	59	27	0.0241
Syne4	Spectrin repeat containing, nuclear envelope family member 4	Microtubule-dependent nuclear positioning	45	70	25	0.0189
Fignl2	Fidgetin-like 2	Unknown	40	63	23	0.0125
Slc5a5	Solute carrier family 5 (sodium iodide symporter), member 5	Regulates iodine uptake in the thyroid	33	51	18	0.0352
Nsmce1	Non-SMC element 1 homolog	Pancreas development	67	81	14	0.0320
Hoxc10	Homeobox C10	Kidney development and limb formation	42	54	12	0.0125
Myo18b	Myosin XVIIIb	Myofibrillar structure maintenance	86	34	52	0.0230
B3gnt8	UDP-GlcNAc:betaGal beta-1,3-*N*-acetylglucosaminyltransferase 8	Positive regulator of cell proliferation	72	32	40	0.0125
P2rx7	Purinergic receptor P2X, ligand-gated ion channel, 7	Neuronal differentiation and migration	79	46	33	0.0244
Dpep1	Dipeptidase 1 (renal)	Kidney and genitourinary development	80	49	31	0.0027
Foxs1	Forkhead box S1	Neuronal differentiation and testicular development	95	64	31	0.0027
Angptl2	Angiopoietin-like 2	Mediates differentiation, migration and inflammation	84	54	30	0.0125
Igfbp6	Insulin-like growth factor binding protein 6	Igf2 signaling	76	46	30	0.0406
Nt5dc2	5′-nucleotidase domain containing 2	Unknown	85	57	28	0.0224
Trim63	Tripartite motif-containing 63	Cardiomyocyte development	69	41	28	0.0352
Ica	RIKEN cDNA 1300017J02 gene	Putative hepatic iron regulator	86	59	27	0.0125
Wdr63	WD repeat domain 63	Gonad development	85	59	27	0.0128

[a]Gene function from NCBI, GeneRIF.
[b]Mean methylation of three mice.
[c]FDR corrected.

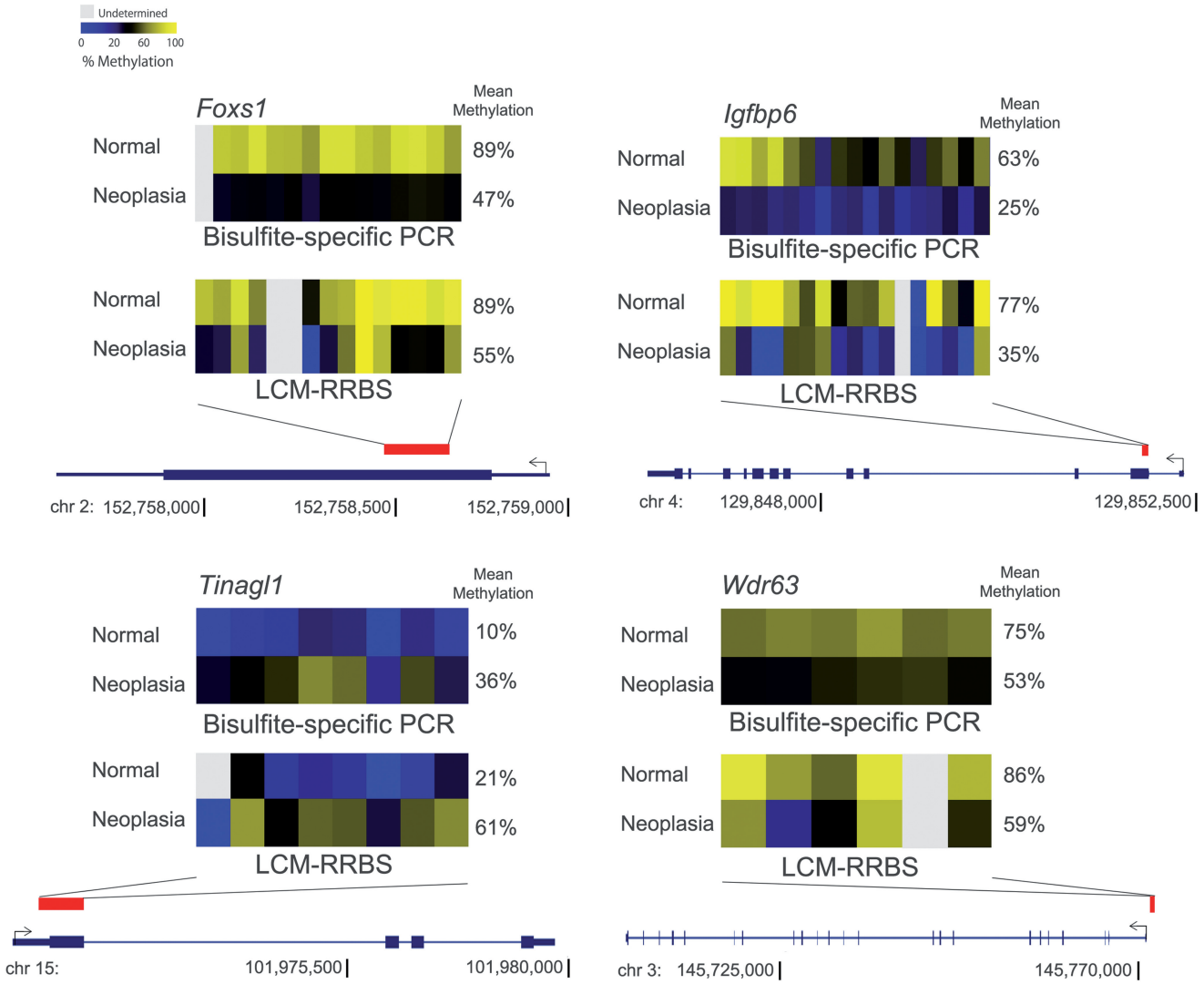

Figure 5. Validation of differentially methylated promoters. The DNA methylation of one hypermethylated and three hypomethylated promoters was interrogated by BSP and sequencing across enriched neoplastic and normal samples. All genes show a statistically significant difference (Fisher's exact test, $P < 10^{-15}$) in DNA methylation using BSP. Each colored box represents an individual CpG dinucleotide within a 2-kb region centered around the TSS. High (yellow), moderate (black), low (blue) and undetermined methylation levels are shown for each CpG. The mean methylation of each region interrogated is shown to the right of each heatmap. The red box indicates the region of the promoter that was interrogated by LCM-RRBS and BSP.

technique, was recently shown to function on 0.5–10 ng of genomic DNA isolated from mouse embryos (34). RRBS, however, has not been demonstrated to function on LCM samples collected from FFPE tissue nor is it amenable to large scale sample processing. We have developed a new method, LCM-RRBS, which can accurately profile genome-wide DNA methylation of many LCM samples in parallel at single base pair resolution.

Our method can be implemented in 3–4 days, and the bulk of the protocol can be automated for high-throughput 96-well experiments. While traditional RRBS requires each processed sample to undergo gel extraction, a laborious process when processing more than a few samples, our method pools all samples together before gel extraction, reducing the required number of gel extractions to one. Thus, a large number of samples can be easily processed at a single time. Furthermore, because high DNA loss results from gel extraction, pooling samples before gel extraction allows the use of low (1 ng) DNA inputs.

The LCM-RRBS protocol affords a significant reduction in sequencing costs compared with whole-genome bisulfite sequencing. We typically collect 1.5 gigabases (GB) per sample, which is considerably less than the ~60 GB needed for 20× coverage of a whole-genome bisulfite library. The sequencing cost per sample can be reduced further if fewer CpGs are interrogated. For example, if a smaller size fraction is isolated during gel extraction, only ~0.75 GB is required per sample.

We found that although formalin fixation and paraffin embedding does not alter DNA methylation *per se*, at least 20 mm^2 of tissue must be isolated for accurate DNA methylation profiling. We were able to create LCM-RRBS libraries from 10, 5 and 2 mm^2 of FFPE tissue and obtained similar numbers of sequencing

reads as with fresh frozen samples, but overall mapping quality was very low (~30% aligned) in the FFPE samples, precluding an accurate analysis of DNA methylation. In contrast, LCM-RRBS generated high-quality methylation maps from 2 mm^2 of microdissected fresh frozen tissue, as demonstrated by our analysis of mouse liver.

To demonstrate the utility of LCM-RRBS, we analyzed the DNA methylation patterns of GDX-induced adrenocortical neoplasms using an average of 5.5 mm^2 of fresh frozen tissue. We hypothesized that aberrant DNA methylation changes could be involved in the formation of these neoplastic tissues. Indeed, recent studies have shown that altered DNA methylation can redirect cell fate in endocrine tissues (49). Conditional mutagenesis of the mouse *Dnmt1* gene, which encodes the maintenance DNA methyltransferase, converts insulin-producing pancreatic β-cells into glucagon-producing α-cells (49). It is thought that because of a common developmental origin, β- and α-cells share general epigenetic programs that provide a compatible environment for cell fate conversions (50). GDX-induced adrenocortical neoplasia may be another example of DNA methylation–regulated cell fate conversion in an endocrine tissue; in this case, adrenocorticoid-producing cells become sex steroid–producing cells (39,51,52). The changes in DNA methylation we observe around the TSS could lead to changes in gene expression (53,54). Several of the genes we found to be differentially methylated in GDX-induced adrenocortical neoplasms have established roles in adrenocortical or gonadal development. For example, *Tinagl1*, a gene implicated in adrenal zonation (55,56), showed a gain in DNA methylation, which could lead to down-regulation. *Wdr63*, *Foxs1* and *Tmem184a*, genes involved in gonadal development (57–60), showed a loss of DNA methylation, which could lead to the aberrant expression of these gonadal-like markers in the adrenal cortex. Furthermore, *Srd5a3*, a gene involved in the biosynthesis of the potent androgen 5α-dihydrotestosterone (61), showed a loss of DNA methylation, which could enhance the ectopic production of sex steroids in the adrenal gland (62). Future studies will explore the role of these methylation changes in the pathogenesis of GDX-induced adrenocortical neoplasia.

In conclusion, LCM-RRBS is a robust cost-effective method for the DNA methylation analysis of heterogeneous tissues. This technique allows the study of tumor evolution and epigenetic heterogeneity *in situ* of <1 ng (~150 cells) and can also be applied to investigate the role of DNA methylation in cell fate specification during tissue development. LCM-RRBS is an important milestone toward highly parallel *in situ* analysis of single cells. We anticipate that this protocol will greatly facilitate the analysis of any sample that contains multiple cell types.

ACCESSION NUMBERS

The GEO accession number is GSE45361.

SUPPLEMENTARY DATA

Supplementary Data are available at NAR Online: Supplementary Tables 1 and 2 and Supplementary Figures 1–6.

ACKNOWLEDGEMENTS

The authors thank Amy Schmidt and Paul Goodfellow for kindly providing endometrial samples and members of the Mitra lab and Gordon lab for thoughtful feedback and suggestions throughout this work; Dietmar Spengler for providing the image of the mouse brain section; Vanessa Ridaura, Constantino Schillebeeckx and Charles Higdon for assistance in creating the figures; and Frank Schoettler of the Vision Research Community Morphology and Imaging Core for assistance with LCM. We thank the Genome Technology Access Center in the Department of Genetics at Washington University of Medicine for help with genomic sequencing.

FUNDING

The National Institutes of Health (NIH) [1R01DA025744 to R.D.M.; 1R01DK075618 to D.B.W.]; The Center is partially supported by NCI Cancer Center Support Grant #P30 CA91842 to the Siteman Cancer Center; ICTS/CTSA Grant #UL1RR024992 from the National Center for Research Resources (NCRR), a component of the NIH, and NIH Roadmap for Medical Research. Funding for open access charge: NIH [1R01DA025744].

Conflict of interest statement. None declared.

REFERENCES

1. Bird,A.P. and Wolffe,A.P. (1999) Methylation-induced repression–belts, braces, and chromatin. *Cell*, **99**, 451–454.
2. Robertson,K.D. (2005) DNA methylation and human disease. *Nat. Rev. Genet.*, **6**, 597–610.
3. Kumari,D. and Usdin,K. (2009) Chromatin remodeling in the noncoding repeat expansion diseases. *J. Biol. Chem.*, **284**, 7413–7417.
4. Chahrour,M., Jung,S.Y., Shaw,C., Zhou,X., Wong,S.T., Qin,J. and Zoghbi,H.Y. (2008) MeCP2, a key contributor to neurological disease, activates and represses transcription. *Science*, **320**, 1224–1229.
5. Jin,B., Tao,Q., Peng,J., Soo,H.M., Wu,W., Ying,J., Fields,C.R., Delmas,A.L., Liu,X., Qiu,J. *et al.* (2008) DNA methyltransferase 3B (DNMT3B) mutations in ICF syndrome lead to altered epigenetic modifications and aberrant expression of genes regulating development, neurogenesis and immune function. *Hum. Mol. Genet.*, **17**, 690–709.
6. Goelz,S.E., Vogelstein,B., Hamilton,S.R. and Feinberg,A.P. (1985) Hypomethylation of DNA from benign and malignant human colon neoplasms. *Science*, **228**, 187–190.
7. Wilson,A.S., Power,B.E. and Molloy,P.L. (2007) DNA hypomethylation and human diseases. *Biochim. Biophys. Acta.*, **1775**, 138–162.
8. Reik,W. and Lewis,A. (2005) Co-evolution of X-chromosome inactivation and imprinting in mammals. *Nat. Rev. Genet.*, **6**, 403–410.
9. Jones,P.A. and Baylin,S.B. (2002) The fundamental role of epigenetic events in cancer. *Nat. Rev. Genet.*, **3**, 415–428.
10. Ryan,R.J. and Bernstein,B.E. (2012) Molecular biology. Genetic events that shape the cancer epigenome. *Science*, **336**, 1513–1514.

11. Stratton,M.R. (2011) Exploring the genomes of cancer cells: progress and promise. *Science*, **331**, 1553–1558.
12. Ley,T.J., Ding,L., Walter,M.J., McLellan,M.D., Lamprecht,T., Larson,D.E., Kandoth,C., Payton,J.E., Baty,J., Welch,J. *et al.* (2010) DNMT3A mutations in acute myeloid leukemia. *N. Engl. J. Med.*, **363**, 2424–2433.
13. Dalgliesh,G.L., Furge,K., Greenman,C., Chen,L., Bignell,G., Butler,A., Davies,H., Edkins,S., Hardy,C., Latimer,C. *et al.* (2010) Systematic sequencing of renal carcinoma reveals inactivation of histone modifying genes. *Nature*, **463**, 360–363.
14. Jiao,Y., Shi,C., Edil,B.H., de Wilde,R.F., Klimstra,D.S., Maitra,A., Schulick,R.D., Tang,L.H., Wolfgang,C.L., Choti,M.A. *et al.* (2011) DAXX/ATRX, MEN1, and mTOR pathway genes are frequently altered in pancreatic neuroendocrine tumors. *Science*, **331**, 1199–1203.
15. Weinberg,R.A. (2007) *The Biology of Cancer*, 1st edn. Garland Science, New York.
16. Shackleton,M., Quintana,E., Fearon,E.R. and Morrison,S.J. (2009) Heterogeneity in cancer: cancer stem cells versus clonal evolution. *Cell*, **138**, 822–829.
17. Dalerba,P., Kalisky,T., Sahoo,D., Rajendran,P.S., Rothenberg,M.E., Leyrat,A.A., Sim,S., Okamoto,J., Johnston,D.M., Qian,D. *et al.* (2011) Single-cell dissection of transcriptional heterogeneity in human colon tumors. *Nat. Biotechnol.*, **29**, 1120–1127.
18. Navin,N., Krasnitz,A., Rodgers,L., Cook,K., Meth,J., Kendall,J., Riggs,M., Eberling,Y., Troge,J., Grubor,V. *et al.* (2010) Inferring tumor progression from genomic heterogeneity. *Genome Res.*, **20**, 68–80.
19. Navin,N., Kendall,J., Troge,J., Andrews,P., Rodgers,L., McIndoo,J., Cook,K., Stepansky,A., Levy,D., Esposito,D. *et al.* (2011) Tumour evolution inferred by single-cell sequencing. *Nature*, **472**, 90–94.
20. Fidler,I.J., Gersten,D.M. and Kripke,M.L. (1979) Influence of immune status on the metastasis of three murine fibrosarcomas of different immunogenicities. *Cancer Res.*, **39**, 3816–3821.
21. Heppner,G.H. (1984) Tumor heterogeneity. *Cancer Res.*, **44**, 2259–2265.
22. Michor,F. and Polyak,K. (2010) The origins and implications of intratumor heterogeneity. *Cancer Prev. Res.*, **3**, 1361–1364.
23. Espina,V., Wulfkuhle,J.D., Calvert,V.S., VanMeter,A., Zhou,W., Coukos,G., Geho,D.H., Petricoin,E.F. 3rd and Liotta,L.A. (2006) Laser-capture microdissection. *Nat. Protoc.*, **1**, 586–603.
24. Laird,P.W. (2010) Principles and challenges of genomewide DNA methylation analysis. *Nat. Rev. Genet.*, **11**, 191–203.
25. Herrmann,A., Haake,A., Ammerpohl,O., Martin-Guerrero,I., Szafranski,K., Stemshorn,K., Nothnagel,M., Kotsopoulos,S.K., Richter,J., Warner,J. *et al.* (2011) Pipeline for large-scale microdroplet bisulfite PCR-based sequencing allows the tracking of hepitype evolution in tumors. *PLoS One*, **6**, e21332.
26. Dietrich,D., Lesche,R., Tetzner,R., Krispin,M., Dietrich,J., Haedicke,W., Schuster,M. and Kristiansen,G. (2009) Analysis of DNA methylation of multiple genes in microdissected cells from formalin-fixed and paraffin-embedded tissues. *J. Histochem. Cytochem.*, **57**, 477–489.
27. Taiwo,O., Wilson,G.A., Morris,T., Seisenberger,S., Reik,W., Pearce,D., Beck,S. and Butcher,L.M. (2012) Methylome analysis using MeDIP-seq with low DNA concentrations. *Nat. Protoc.*, **7**, 617–636.
28. Serre,D., Lee,B.H. and Ting,A.H. (2010) MBD-isolated genome sequencing provides a high-throughput and comprehensive survey of DNA methylation in the human genome. *Nucleic Acids Res.*, **38**, 391–399.
29. Brinkman,A.B., Simmer,F., Ma,K., Kaan,A., Zhu,J. and Stunnenberg,H.G. (2010) Whole-genome DNA methylation profiling using MethylCap-seq. *Methods*, **52**, 232–236.
30. Irizarry,R.A., Ladd-Acosta,C., Carvalho,B., Wu,H., Brandenburg,S.A., Jeddeloh,J.A., Wen,B. and Feinberg,A.P. (2008) Comprehensive high-throughput arrays for relative methylation (CHARM). *Genome Res.*, **18**, 780–790.
31. Ball,M.P., Li,J.B., Gao,Y., Lee,J.H., LeProust,E.M., Park,I.H., Xie,B., Daley,G.Q. and Church,G.M. (2009) Targeted and genome-scale strategies reveal gene-body methylation signatures in human cells. *Nat. Biotechnol.*, **27**, 361–368.
32. Diep,D., Plongthongkum,N., Gore,A., Fung,H.L., Shoemaker,R. and Zhang,K. (2012) Library-free methylation sequencing with bisulfite padlock probes. *Nat. Methods*, **9**, 270–272.
33. Lister,R., Pelizzola,M., Dowen,R.H., Hawkins,R.D., Hon,G., Tonti-Filippini,J., Nery,J.R., Lee,L., Ye,Z., Ngo,Q.M. *et al.* (2009) Human DNA methylomes at base resolution show widespread epigenomic differences. *Nature*, **462**, 315–322.
34. Smith,Z.D., Chan,M.M., Mikkelsen,T.S., Gu,H., Gnirke,A., Regev,A. and Meissner,A. (2012) A unique regulatory phase of DNA methylation in the early mammalian embryo. *Nature*, **484**, 339–344.
35. Bielinska,M., Kiiveri,S., Parviainen,H., Mannisto,S., Heikinheimo,M. and Wilson,D.B. (2006) Gonadectomy-induced adrenocortical neoplasia in the domestic ferret (Mustela putorius furo) and laboratory mouse. *Vet. Pathol.*, **43**, 97–117.
36. Bernichtein,S., Petretto,E., Jamieson,S., Goel,A., Aitman,T.J., Mangion,J.M. and Huhtaniemi,I.T. (2008) Adrenal gland tumorigenesis after gonadectomy in mice is a complex genetic trait driven by epistatic loci. *Endocrinology*, **149**, 651–661.
37. Krachulec,J., Vetter,M., Schrade,A., Lobs,A.K., Bielinska,M., Cochran,R., Kyronlahti,A., Pihlajoki,M., Parviainen,H., Jay,P.Y. *et al.* (2012) GATA4 is a critical regulator of gonadectomy-induced adrenocortical tumorigenesis in mice. *Endocrinology*, **153**, 2599–2611.
38. Bielinska,M., Parviainen,H., Kiiveri,S., Heikinheimo,M. and Wilson,D.B. (2009) Review paper: origin and molecular pathology of adrenocortical neoplasms. *Vet. Pathol.*, **46**, 194–210.
39. Bielinska,M., Genova,E., Boime,I., Parviainen,H., Kiiveri,S., Leppaluoto,J., Rahman,N., Heikinheimo,M. and Wilson,D.B. (2005) Gonadotropin-induced adrenocortical neoplasia in NU/J nude mice. *Endocrinology*, **146**, 3975–3984.
40. Gertz,J., Varley,K.E., Reddy,T.E., Bowling,K.M., Pauli,F., Parker,S.L., Kucera,K.S., Willard,H.F. and Myers,R.M. (2011) Analysis of DNA methylation in a three-generation family reveals widespread genetic influence on epigenetic regulation. *PLoS Genet.*, **7**, e1002228.
41. Li,H., Ruan,J. and Durbin,R. (2008) Mapping short DNA sequencing reads and calling variants using mapping quality scores. *Genome Res.*, **18**, 1851–1858.
42. Xi,Y., Bock,C., Muller,F., Sun,D., Meissner,A. and Li,W. (2012) RRBSMAP: a fast, accurate and user-friendly alignment tool for reduced representation bisulfite sequencing. *Bioinformatics*, **28**, 430–432.
43. Rhead,B., Karolchik,D., Kuhn,R.M., Hinrichs,A.S., Zweig,A.S., Fujita,P.A., Diekhans,M., Smith,K.E., Rosenbloom,K.R., Raney,B.J. *et al.* (2010) The UCSC genome browser database: update 2010. *Nucleic Acids Res.*, **38**, D613–D619.
44. Gardiner-Garden,M. and Frommer,M. (1987) CpG islands in vertebrate genomes. *J. Mol. Biol.*, **196**, 261–282.
45. Pruitt,K.D., Tatusova,T., Brown,G.R. and Maglott,D.R. (2012) NCBI Reference Sequences (RefSeq): current status, new features and genome annotation policy. *Nucleic Acids Res.*, **40**, D130–D135.
46. Gu,H., Bock,C., Mikkelsen,T.S., Jager,N., Smith,Z.D., Tomazou,E., Gnirke,A., Lander,E.S. and Meissner,A. (2010) Genome-scale DNA methylation mapping of clinical samples at single-nucleotide resolution. *Nat. Methods*, **7**, 133–136.
47. Warnecke,P.M., Stirzaker,C., Melki,J.R., Millar,D.S., Paul,C.L. and Clark,S.J. (1997) Detection and measurement of PCR bias in quantitative methylation analysis of bisulphite-treated DNA. *Nucleic Acids Res.*, **25**, 4422–4426.
48. Morohashi,K. and Zubair,M. (2011) The fetal and adult adrenal cortex. *Mol. Cell. Endocrinol.*, **336**, 193–197.
49. Dhawan,S., Georgia,S., Tschen,S.I., Fan,G. and Bhushan,A. (2011) Pancreatic beta cell identity is maintained by DNA methylation-mediated repression of Arx. *Dev. Cell*, **20**, 419–429.
50. Akerman,I., van Arensbergen,J. and Ferrer,J. (2011) Removing the brakes on cell identity. *Dev. Cell*, **20**, 411–412.
51. Johnsen,I.K., Slawik,M., Shapiro,I., Hartmann,M.F., Wudy,S.A., Looyenga,B.D., Hammer,G.D., Reincke,M. and Beuschlein,F. (2006) Gonadectomy in mice of the inbred strain CE/J induces proliferation of sub-capsular adrenal cells expressing gonadal marker genes. *J. Endocrinol.*, **190**, 47–57.

52. Bielinska,M., Parviainen,H., Porter-Tinge,S.B., Kiiveri,S., Genova,E., Rahman,N., Huhtaniemi,I.T., Muglia,L.J., Heikinheimo,M. and Wilson,D.B. (2003) Mouse strain susceptibility to gonadectomy-induced adrenocortical tumor formation correlates with the expression of GATA-4 and luteinizing hormone receptor. *Endocrinology*, **144**, 4123–4133.
53. Brenet,F., Moh,M., Funk,P., Feierstein,E., Viale,A.J., Socci,N.D. and Scandura,J.M. (2011) DNA methylation of the first exon is tightly linked to transcriptional silencing. *PLoS One*, **6**, e14524.
54. Hartung,T., Zhang,L., Kanwar,R., Khrebtukova,I., Reinhardt,M., Wang,C., Therneau,T.M., Banck,M.S., Schroth,G.P. and Beutler,A.S. (2012) Diametrically opposite methylome-transcriptome relationships in high- and low-CpG promoter genes in postmitotic neural rat tissue. *Epigenetics*, **7**, 421–428.
55. Mukai,K., Mitani,F., Nagasawa,H., Suzuki,R., Suzuki,T., Suematsu,M. and Ishimura,Y. (2003) An inverse correlation between expression of a preprocathepsin B-related protein with cysteine-rich sequences and steroid 11beta -hydroxylase in adrenocortical cells. *J. Biol. Chem.*, **278**, 17084–17092.
56. Li,D., Mukai,K., Suzuki,T., Suzuki,R., Yamashita,S., Mitani,F. and Suematsu,M. (2007) Adrenocortical zonation factor 1 is a novel matricellular protein promoting integrin-mediated adhesion of adrenocortical and vascular smooth muscle cells. *FEBS J.*, **274**, 2506–2522.
57. Sato,Y., Baba,T., Zubair,M., Miyabayashi,K., Toyama,Y., Maekawa,M., Owaki,A., Mizusaki,H., Sawamura,T., Toshimori,K. *et al.* (2008) Importance of forkhead transcription factor Fkhl18 for development of testicular vasculature. *Mol. Reprod. Dev.*, **75**, 1361–1371.
58. Svingen,T., Beverdam,A., Bernard,P., McClive,P., Harley,V.R., Sinclair,A.H. and Koopman,P. (2007) Sex-specific expression of a novel gene Tmem184a during mouse testis differentiation. *Reproduction*, **133**, 983–989.
59. Best,D., Sahlender,D.A., Walther,N., Peden,A.A. and Adams,I.R. (2008) Sdmg1 is a conserved transmembrane protein associated with germ cell sex determination and germline-soma interactions in mice. *Development*, **135**, 1415–1425.
60. Bonilla,E. and Xu,E.Y. (2008) Identification and characterization of novel mammalian spermatogenic genes conserved from fly to human. *Mol. Hum. Reprod.*, **14**, 137–142.
61. Uemura,M., Tamura,K., Chung,S., Honma,S., Okuyama,A., Nakamura,Y. and Nakagawa,H. (2008) Novel 5 alpha-steroid reductase (SRD5A3, type-3) is overexpressed in hormone-refractory prostate cancer. *Cancer Sci.*, **99**, 81–86.
62. Payne,A.H. and Hales,D.B. (2004) Overview of steroidogenic enzymes in the pathway from cholesterol to active steroid hormones. *Endocr. Rev.*, **25**, 947–970.